POLITECNICO DI TORINO
Repository ISTITUZIONALE

Multi-objective optimisation of an aerostatic pad: design of position, number and diameter of the supply holes

Original
Multi-objective optimisation of an aerostatic pad: design of position, number and diameter of the supply holes / Colombo, F., Della Santa, F., Pieraccini, S.. - In: JOURNAL OF MECHANICS. - ISSN 1727-7191. - 36:3(2020), pp. 347-360. [10.1017/jmech.2019.41]

Availability:
This version is available at: 11583/2743224 since: 2020-06-18T10:14:02Z

Publisher:
Cambridge University Press

Published
DOI:10.1017/jmech.2019.41

Terms of use:

This article is made available under terms and conditions as specified in the corresponding bibliographic description in the repository

Publisher copyright

(Article begins on next page)

29 November 2026

MULTI-OBJECTIVE OPTIMISATION OF AN AEROSTATIC PAD: DESIGN OF POSITION, NUMBER AND DIAMETER OF THE SUPPLY HOLES

F. Colombo

Department of Mechanical and Aerospace Engineering,
Politecnico di Torino
Torino, Italy

F. Della Santa

Department of Mathematical Sciences
Politecnico di Torino
Torino, Italy

SmartData@PoliTO
Politecnico di Torino
Torino, Italy

S. Pieraccini

Department of Mechanical and Aerospace Engineering
Politecnico di Torino
Torino, Italy

Member of the INdAM research group GNCS

ABSTRACT

In this paper, a rectangular aerostatic bearing with multiple supply holes is optimised with a multi-objective optimisation approach. The design variables taken into account are the supply holes position, their number and diameter, the supply pressure, while the objective functions are the load capacity, the air consumption and the stiffness and damping coefficients. A genetic algorithm is applied in order to find the Pareto set of solutions. The novelty with respect to other optimisations which can be found in literature is that number and location of the supply holes is completely free and not associated to a pre-defined scheme. A vector x associated with the supply holes location is introduced in the design parameters and given in input to the optimizer.

Keywords: Multi-objective optimisation, gas lubrication, genetic algorithm.

Many applications, which require low friction motion, employ gas bearings. These applications interest two main fields: the high speed and the high precision sectors. For a good design of the components, it is essential to have sufficiently accurate numerical models that allow a good estimation of their static and dynamic characteristics.

The gas bearing design is often driven by the necessity of maximizing a parameter, such as the load capacity, the stiffness, the damping capability, the stability margin or minimizing the air consumption, the friction coefficient and the power losses. In literature, there are many works on this topic, with the aim of choosing the best geometry of a journal bearing, an axial thrust bearing or a slider.

The geometrical design variables can regard i) the supply system, such as orifices, grooves, slots or porous areas, ii) the shape of the air gap, such as the conicity of the gap in aerostatic pads [1] or the profile of waved journal bearings [2] or iii) the topology of the slider in near contact recording field [3].

Ref. [4] optimises the size of porous material regions of square shape in order to maximize the bearing stiffness and minimize the air consumption simultaneously. The same geometry is re-designed in [5] considering the Pareto fronts of the load capacity vs stiffness and of the air consumption vs stiffness.

A spiral groove dynamic thrust bearing is designed to maximize the stiffness in [6]. In this case, the generally used logarithmic spiral is modified with a spline function. Refs. [7, 8] optimise a spiral groove thrust bearing and the herringbone grooved journal bearings for maximizing the dynamic stability and for minimizing the windage losses in a heat pump turbocompressor.

* Corresponding author (federico.colombo@polito.it, phone: +390110906567, fax: +390110906999)

In hard disk drives (HDD) technology, different studies on the shape of the slider have been conducted, such as in [3, 9, 10]. The purpose is to have a stiff bearing in order to guarantee a constant flying height over the entire disk. The optimisation algorithm is aimed to optimise the air bearing contour for optimum shock response in [11]. Paper [12] considers the optimisation of the head shape of a video tape recorder, in which the rotation of the drum creates an air film between the magnetic medium and the head. To this purpose, a genetic algorithm is developed in conjunction with finite element method.

Focusing the attention on the optimisation methods used in gas lubrication problems, researchers have developed different strategies. Evolutionary methods, such as genetic algorithm (GA) methods, take advantage of parallel computing, as they need to perform many simulations independently. The genetic algorithm was firstly used in 60s and 70s, see [13], while the first multi-objective GA, called Vector Evaluated Genetic Algorithm, was proposed in 80s in [14]. Then, many evolutionary algorithms for multi-objective optimization were proposed, see e.g. [15-22].

Regarding gas bearings optimization, Ref. [23] adopts this strategy to solve a multi-objective optimisation problem. Paper [24] uses a multi-objective optimiser based on evolutionary algorithms to maximize the stability and minimize the power losses of herringbone grooved gas bearings supporting a high-speed rotor. GA is also used in the topology optimisation of the hard disk driver (HDD) slider [25]; the genetic algorithm is employed for the determination of the optimal solution from the possible candidates. A hybrid approach is used in [26] to optimise a porous air bearing: the genetic algorithm is used as an initial method for few generations; the simplex method is then activated and applied until a solution is found. An optimisation method using non-dominated sorting genetic algorithm (NSGA) is applied for a two-objective optimisation to achieve a minimum air consumption and maximum load capacity in [27]. Simulated annealing is used in Ref. [28] for the design of a sub-25 nm fly height slider for near contact recording applications. Paper [29] adopts the sequential quadratic programming (SQP) method in order to meet the desired flying characteristics of the slider over the entire recording band. A deterministic global optimisation technique is employed in [30] for the slider surface design in HDD.

In metrology, there is the need of optimising the geometry of the aerostatic bearings that sustain the measuring machine. For example Refs. [31, 32] consider a multi-orifice pad and optimise the number and diameter of supply orifices positioned along two lines in order to minimize the inverse of the load, the inverse of stiffness and the flow. In [33] a rectangular aerostatic pad with multiple supply holes is studied and the effect of design variables on the static performance is evaluated with a multi-objective optimisation approach based on genetic algorithms. Anyway, only static characteristics of the pad are considered and the geometry is limited by the localization of the supply holes along a rectangular perimeter.

In order to emancipate from a fixed scheme in which the supply holes are positioned, the present paper examines a rectangular pad letting to the optimiser to choose number and position of the supply holes. This is a novelty, as in literature can be found optimizations in which the supply holes are *a-priori* positioned following a given scheme, e.g. at a given distance from the pad edges like in [33], or along two or three rows like in [31, 32]. To the best of the authors' knowledge, there are no works in literature dealing with the optimization of aerostatic pads endowed of supply holes whose number and position is completely free. Moreover, the analysis entails not only the static characteristics of the pad, such as the load capacity and the air consumption, but also the stiffness and damping coefficients.

The objectives of maximizing load capacity, stiffness and damping capability and minimizing the air consumption are conflicting. One possibility to solve this problem is to define a linear combination of these objective functions with given weighting factors, but the results are quite sensitive to the chosen weights. As an alternative, the multi-objective approach can be considered, treating the objectives as equal entities and providing distortion-free information about the ideal trade-off between the objectives. The Pareto front shows many available solutions from which the designer can select the best trade-off among the possible conflicting objective functions. For this reason, in this paper the multi-objective procedure is adopted in order to visualize the ideal trade-off between the conflicting objectives and let the engineer to make decision about the final design.

2. MODEL DESCRIPTION

For the reader's convenience, in this section the model used is briefly recalled. The numerical model has been validated through an extensive experimental campaign, as described in [34].

A rectangular pad of dimensions L_x and L_y along x and y directions is considered. The number of the supply holes, their diameter and their position are parameters to be determined by means of the optimisation process. A uniform mesh is considered, with n and m nodes along x and y directions respectively. Reynolds equation (1) for gas lubricated films is discretized with finite differences under the assumption of isothermal flow expansion:

$$\frac{\partial}{\partial x}\left(\frac{ph^3}{\mu}\frac{\partial p}{\partial x}\right)+\frac{\partial}{\partial y}\left(\frac{ph^3}{\mu}\frac{\partial p}{\partial y}\right)=12\frac{\partial(ph)}{\partial t} \tag{1}$$

where p is the pressure, h is the air gap under the pad, and μ the air viscosity. In case of presence of the supply hole, the mass balance equation (2) in the controlled volume is considered, see Figure 1:

$$\oint_{\Gamma_{i,j}} (ph^3 \nabla p) \cdot ndl + 12\mu RT G_{in} = 12\mu \frac{\partial}{\partial t} \iint_{\Sigma_{i,j}} phdxdy \tag{2}$$

where $\Gamma_{i,j}$ is the boundary of the control volume around node (i,j), $\Sigma_{i,j}$ is the surface of the control volume, T is the temperature, R is the gas constant equal to 287 J/(kg K), and G_{in} is the mass flow through the supply hole. Eq. (2) is discretized with finite difference technique using a mesh of 50x75 elements.

In sonic conditions the input flow is given by:

$$G_{in} = c_1 k_T c_d p_s \tag{3}$$

where k_T depends on the temperature ratio and is defined as $k_T = \sqrt{T_0/T}$, c_1 is the conductance, given by

$$c_1 = \frac{0.685}{\sqrt{RT}} \frac{\pi d_s^2}{4} \tag{4}$$

and d_s is the supply holes diameter. Standard condition is defined as T0=293.5 K and p_0=100 kPa. In subsonic conditions the flow is

$$G_{in} = c_1 k_T c_d p_s \sqrt{1 - \phi^2} \tag{5}$$

where the pressure ratio ϕ is

$$\phi = \frac{p_c/p_s - b}{1 - b} \tag{6}$$

being p_c the supply holes downstream pressure, p_s the input air pressure, and b the critical pressure ratio. Discharge coefficient c_d is defined using an experimentally obtained formula, see [35]. As stated in the mentioned paper, this coefficient relates the experimental air flow that crosses the supply orifice with the theoretical air flow, calculated in the isentropic expansion condition. Therefore, eq. (7) is used to calculate the discharge coefficient:

$$c_d = 0.85\left(1 - e^{-8.2h/d_s}\right) \tag{7}$$

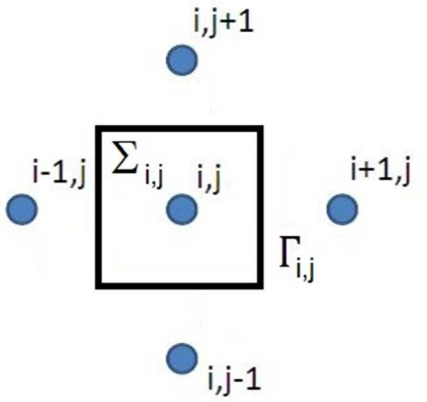

Fig. 1 5 points stencil around the control volume centered in (i,j).

Let c denote the damping, k the stiffness, F the load capacity and G the mass air flow. Stiffness and damping coefficients are obtained supposing a small sinusoidal perturbation of the air gap ($\Delta h = 0.5\ \mu m$) at a given frequency ω around the steady operating point

$$h = h_s + \Delta h sin\omega t \tag{8}$$

and calculating the resulting bearing force

$$F = F_s + \Delta F sin(\omega t + \phi) \tag{9}$$

where ϕ is the phase lag between F and h. ΔF depends on the pad stiffness; it ranges from 20 to 100 N.

The coefficients are then computed by

$$k = \frac{-\Delta F cos\phi}{\Delta h} \tag{10}$$

$$c = \frac{-\Delta F sin\phi}{\omega \Delta h} \tag{11}$$

The following dimensionless parameters are then defined:

$$\bar{\mathrm{h}} = \frac{h}{h_{ref}}, \qquad \bar{\mathrm{d}} = \frac{d}{d_{ref}}, \qquad \bar{\mathrm{G}} = \frac{G}{G_\infty}$$

$$\bar{\mathrm{F}} = \frac{F}{p_a L_x L_y}, \qquad \bar{\mathrm{k}} = \frac{k h_{ref}}{p_a L_x L_y}, \qquad \bar{\mathrm{c}} = \frac{c h_{ref}^3}{12 \mu L_x^3 L_y}$$

where G_1 is the air flow of a reference pad at infinite air gap, while h_{ref}, d_{ref} are the reference values for the air gap and the supply holes diameter. G_1 is calculated considering the reference supply holes diameter d_{ref}, a reference value for the supply pressure $p_{\mathrm{s,ref}}=7\cdot10^5$ Pa, and a reference holes number $N_{\mathrm{ref}}=60$.

3. DESCRIPTION OF THE OPTIMISATION APPROACH

In this section the optimisation framework followed herein is described. The target is to automatically design an optimal pad (namely, to automatically detect an optimal number and distribution of holes, and an optimal supply pressure) by simultaneously maximizing damping, stiffness, load capacity, and minimizing mass air flow. The target is pursued by using a multi-objective optimisation approach. In the next section the objective functions and the design parameters are introduced.

3.1 Optimisation problem

The following objective functions are considered:

- f_1=-c (the opposite of the damping coefficient);
- f_2=-k (the opposite of the stiffness coefficient);
- f_3=-F (the opposite of the load capacity);
- f_4=G (the mass air flow).

The following design parameters are introduced:

1. $p_s \in R$ is the input air pressure; it is assumed to be a continuous variable;
2. $x \in \{0,1\}^q \subset R^q$ is a vector of q unknowns representing possible presence of holes in the reduced pad; assuming that the nodes of the mesh grid are denoted by P_l, l=1,…,q=n·m, each component x_l of x is a binary variable, namely x_l=1 represents the hole presence at point P_l, whereas x_l=0 means that no hole is present at P_l;
3. $d \in R^q$ is a vector whose component d_l, l=1…q, represents the diameter of a possible hole in position P_l; each component is assumed to be a continuous variable.

The design variables are collected in a vector $y = (p_s, d, x)^T \in R^{1+2q}$. Note that since variables x_l are binary, one immediately has that the sum of all these binary variables equals the number of holes N_h:

$$\sum_{l=1}^{q} x_l = N_h \tag{12}$$

Suitable constraints are imposed on the design variables, namely:

1. bound constraints are imposed both on p_s and on d: $p_{\min} \le p_s \le p_{\max}$, $d_{\min} \le d_l \le d_{\max}$ where $p_{\min}$, $p_{\max}$ ($d_{\min}$, $d_{\max}$) represent lower and upper bounds on p_s (on d_l, respectively);
2. a minimum and a maximum number of holes is also considered, through the constraint

$$N_{min} \le \sum_{l=1}^{q} x_l \le N_{max} \tag{13}$$

As a whole, there are therefore a two-sided linear constraint and bound constraints on all the variables (note that also the binary variables are in fact bound constrained by the values 0 and 1). The problem is rewritten as:

$$\min_{y \in R^{1+2q}} \left(f_1(y), f_2(y), f_3(y), f_4(y)\right) \tag{14}$$

subject to $Ay \le b$, $L \le y \le U$, where $A \in R^{2\times(1+2q)}$ and $b \in R^2$ are introduced to rewrite (12) in the matrix form $Ay \le b$, and $L, U \in R^{1+2q}$ are vectors collecting the lower and upper bounds, respectively. The bound constraints $L \le y \le U$ are meant component-wise.

Problem (13) is a multi-objective optimisation problem, in which one seeks a solution which simultaneously minimizes all the given objective functions $f_1,\ldots,f_4$. If the objective functions f_i have a conflicting behaviour, a y value that simultaneously minimizes all objectives may fail to exist and the so-called *Pareto optimal solutions* are sought instead.

Pareto optimal solutions of a problem of type (13) consist in a set Y_P of vectors $y^* \in R^{1+2q}$ such that none of the corresponding values for the objective functions $f_1(y^*), f_2(y^*), f_3(y^*), f_4(y^*)$ can be further reduced without increasing some of the other ones. In other words, for each $y^* \in Y_P$ and for each $y \in R^{1+2q}$, if there exists $i \in \{1,\ldots,4\}$ such that $f_i(y) \leq f_i(y^*)$, then there also exists $j \neq i$, $j \in \{1,\ldots,4\}$, such that $f_j(y^*) \leq f_j(y)$. Elements of set Y_P are also called non-dominated or rank 1 individuals. Furthermore, for each $n \geq 2$, a vector $y \in R^{1+2q}$ is said to have rank n if it is dominated only by vectors with rank lower than n.

Figure 2 depicts an example of a typical representation of Pareto optimal solutions for a hypothetical problem with two conflicting objective functions f_1 and f_2. The plot is reported in the (f_1, f_2) plane, and the dots correspond to possible outputs of simulations. Among such points, the red dots correspond to Pareto optimal solutions; this set of points is also called Pareto's front. The black dots correspond to non-optimal points, namely, points for which some improvement can still be obtained on at least one of the two objectives without compromising the other.

In the next section the approach adopted to solve the mixed-integer multi-objective optimisation problem (13) using a genetic algorithm is sketched; the results obtained are discussed in section 4.

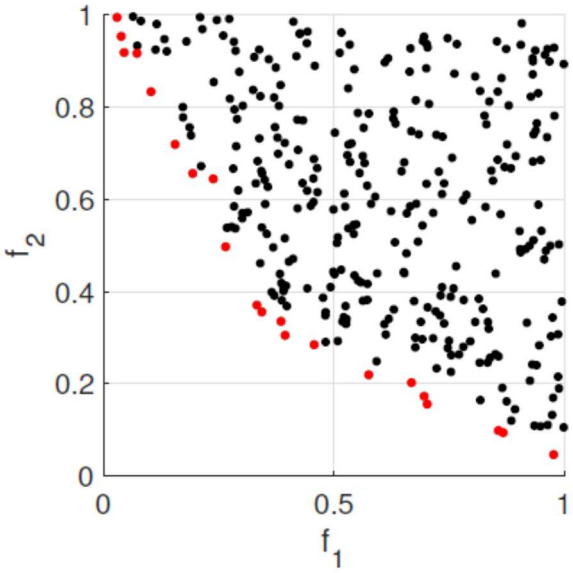

Fig. 2 Example of Pareto optimal solutions. Red dots: optimal solutions (Pareto Front); black dots: non-optimal points.

3.2 Numerical implementation

Term *Genetic algorithms* (GA) refers to a family of derivative-free optimisation algorithms inspired by biological evolution process, that can be applied both in mono-objective and multi-objective optimisation. In general, these kinds of algorithms consist in an iterative process that, starting from a random set of points, at iteration k+1, k≥0, computes a new set of points, called (k+1)-th generation, that is closer to the minimizer (mono-objective optimisation) or to the Pareto front (multi-objective optimisation) than the points of previous generation are. Given the multi-objective optimisation problem (13), a multi-objective GA performs the optimisation process as follows [36, p.9]:

1. **Initial population:** the algorithm creates an initial random population $G_0 = \left\{y_1^{(0)}, \ldots, y_N^{(0)}\right\}$ (Generation 0) with all elements, or most of them, satisfying the given constraints;
2. **Evolution:** let G_k be the last generation computed, then a new generation $G_{k+1} = \left\{y_1^{(k+1)}, \ldots, y_N^{(k+1)}\right\}$ is created from the population of G_k. Given a fixed fraction parameter $p \in (0, 1)$, a number of elements equal to $p \cdot N$ is generated using a *crossover* operation, creating a set X_k, while $(p - 1) \cdot N$ elements are generated with a *mutation* operation, creating a set M_k. These operations are such that:

a. **Crossover:** the set X_k is arbitrarily created from information of pairs of elements in G_k chosen with respect to an arbitrary selection criterion (elements in X_k are then called "crossover children" and the couples of selected elements are called "parents");
b. **Mutation:** the set M_k is created by perturbing, with respect to a given rule, some elements in G_k selected with the same criterion used for parents of X_k (elements in M_k are then called "crossover children").

Once computed X_k and M_k , an "extended population" $\overline{G_k} = G_k \cup X_k \cup M_k$ is considered and G_{k+1} is obtained trimming $\overline{G_k}$ to have N elements by retaining a suitable number of individuals of each rank.

3. **Iteration or stop:** a fraction of elements of the "local" Pareto front of G_{k+1} (namely, the set of rank 1 elements of G_{k+1}) are selected with respect to a "crowding" distance measure. If these subset of elements P_{k+1} does not significantly improve on the one of G_k (with respect to a spread measure), then the algorithm returns $P^* = P_{k+1}$ as Pareto's front. Else, the algorithm continues from step 2.

The numerical experiments reported herein are obtained using the MATLAB routine `gamultiobj`, a function that finds the Pareto front of multiple cost functions using a genetic algorithm. All details about parents selection, crowding distance and spread measure used by `gamultiobj` are described in [36, p.6-10] and [37, p.43-45]. The value used for parameter p was 0.8 (default option) and the number of rank 1 elements chosen at step 3 is equal to the minimum value between $0.35 \cdot N$ and their total number (default option).

In MATLAB genetic algorithms `ga` and `gamultiobj` (for mono-objective and multi-objective optimisation, respectively) the user may choose between some default, general-purpose creation, mutation and crossover functions, which allow to set the criteria under-pinning steps 1, 2.a. and 2.b.. The optimisation problem (13) is a mixed-integer optimisation problem with linear and bound constraints. Since function `gamultiobj`, unlike `ga`, is not designed for managing mixed-integer problems, none of the default, general-purpose built-in functions available in MATLAB was well-suited for tackling problem (13), and most of them was even not applicable. The design of new functions, tailored on the specific problem (13), represented a further step towards the improvement of the overall behaviour of the algorithm.

Hence, new functions have been created, tailored on the mixed-integer multi-objective optimisation problem described in previous sections. The new functions introduced are the following:

Creation Function: The tailored creation function has been built from scratch. This function creates a population of random vectors $G_0 = \left\{y_1^{(0)}, \dots, y_N^{(0)}\right\} \subset R^{1+2q}$ such that, for each $y = (p_s, d, x) \in G_0$ it is:

- p_s randomly chosen from a continuous uniform distribution on $[p_{min}, p_{max}]$;
- x a binary vector in R^q with an initial number of elements set to 1 that is equal to the (rounded) average of N_{min} and N_{max}; the elements to be set equal to 1 are uniformly randomly chosen;
- d is first built as a uniform random vector in R^q, with entries randomly chosen between d_{min} and d_{max}. Then, for each l such that $x_l = 0$, the corresponding diameter d_l is set to 0.

Mutation function: The tailored mutation function modifies the standard MATLAB function `mutationadaptfeasible.m` generating elements in M_k that satisfy bounds and linear constraints. Then the components of $y = (p_s, d, x) \in M_k$ corresponding to x are rounded to transform them in binary variables; finally, if some x_l is equal to 0, the function sets the corresponding diameter d_l to 0.

Crossover function: The tailored crossover function modifies the standard MATLAB function `crossoverintermediate.m`. The new function creates a set X_k of children by taking a weighted average of the parents such that, for each $y' \in X_k$ with parents y_1, y_2, we have $y' = (1 - r)y_1 + ry_2$, being r a uniform random number in [0, 1]. Then, for each $y' = (p_s', d', x') \in X_k$ it rounds vector's components $x' = \left(y'_{1+q+1}, \dots, y'_{1+2q}\right)$ to values 0 or 1 and, if some $x_l' = 0$, it sets the corresponding diameter d_l' to 0.

4. ANALYSIS OF THE RESULTS

The results of the optimisation are here presented in dimensionless form (see section 2). The bounds of the design parameters are selected on the base of the commonly used values in applications. They are specified by $N_{min} = 4$ and $N_{max} = 60$, $p_{min} = 4.5 \cdot 10^5$ Pa and $p_{max} = 7 \cdot 10^5$ Pa, $\bar{d}_{min} = 0.5$ and $\bar{d}_{max} = 4$. The objective functions are calculated at $\bar{h} = 0.8$, while stiffness and damping coefficients are calculated perturbing the air gap around the static value with a sinusoid of amplitude $\delta\bar{h} = 0.05$ and frequency $f = 100$ Hz. As far as GA parameters are concerned, the population size, at each generation, was set to 350 elements and two stopping criteria have been used: a maximum number of 500 generations and a tolerance equal to 10^{-4} for the average change in the spread of Pareto solutions.

Two cases were analysed: in the first one, the presence of a supply hole in the center of the pad was forced; in the

second one, the possibility of positioning a supply hole in the center or not was given to the genetic algorithm.

The rank 1 elements of the last generation are 144 out of 350 members of the population in the first case and 149 out of 350 in the second case; However, in the Pareto sets returned by the algorithm are present $123 \approx 0.35 \cdot 350$ configurations for each case, due to the reasons described at the step 3 of Section 3.2. In both cases the solution presents some recurrent holes disposition, which are characterized by different supply pressure and mean holes diameter. Authors have noticed that when the central hole is forced (first case) its diameter is much greater than the diameter of the other holes. In this case, the other holes are quite far from the central hole. Moreover, when the central hole is not forced (second case), the central hole is never present.

4.1 Analysis of the Pareto front

The 4D Pareto fronts obtained in the optimisation process in the two cases of central hole forced or not are reported in Figure 3.
In such figure, the Pareto front is plotted in the f_1, f_2, f_3 space, while the air consumption is represented by means of the colour scale. The Pareto fronts have a similar helical shape in both cases. The average holes diameter obtained within the optimisation process is also represented in this figure by means of the dots diameter, which is proportional to the mean diameter of the supply holes. It can be noticed that the mean diameter increases moving on the Pareto front towards higher load capacity and air consumption of the pad.

In Figure 4 the same 4D Pareto fronts are visualized with also the non-optimal individuals (more than one half of the population) obtained at the last generation.

In order to better understand possible correlations among the design parameters under investigation, some 2D projections of the Pareto front are depicted in Figure 5. The following considerations can be deduced from these projections:

- on the Pareto front an increase on the load capacity corresponds to an increase of air consumption and damping coefficient (see top and bottom panels, respectively);
- maximum stiffness is obtained at an average load capacity; if the load capacity is increased or decreased from this point, stiffness is decreased (middle panels);
- it is impossible to simultaneously maximize both damping and stiffness, as damping increases with load capacity, whereas stiffness has a non-monotonic behaviour with respect to load capacity.

The high variation of the objective functions is mainly due to the change in supply pressure, but also the mean diameter, the number and the disposition of the supply holes have a non-negligible influence.

4.2. Comparison of configurations at the same supply pressure

In order to deduce the effect of the holes location on the pad performance, some example elements of the Pareto set displaying approximately the same supply pressure are selected for a comparison. Considering the first case (central hole forced), configurations 85, 103 and 111 have supply pressure around 6 bar. Table 1 reports the mean diameter of the supply holes, the standard deviation of the diameters distribution, the supply pressure and the number of holes together with the values of the four objective functions. In Figure 6 are also depicted the holes dispositions, with dots size proportional to the supply hole diameter. In Figure 7 the objective functions are represented vs the air gap $\bar{h}$. These graphs complete the data provided in Table 1, which are valid at $\bar{h}$= 0.8.

Table 1 Example of comparison of three configurations at similar supply pressure, with central hole forced.

Configuration	**85**	**103**	**111**
Mean diameter $\bar{d}$	0.85	0.87	1.01
Standard deviation	0.41	0.47	0.43
Number of holes	37	35	41
Supply pressure (bar)	6.018	6.017	6.018
Load capacity $\bar{F}$ (at $\bar{h} = 0.8$)	2.724	2.870	3.056
Airflow $\bar{G}$ (at $\bar{h} = 0.8$)	0.143	0.078	0.177
Stiffness $\bar{k}$ (at $\bar{h} = 0.8$)	2.93	1.36	2.38
Damping $\bar{c}$ (at $\bar{h} = 0.8$)	0.0116	0.0117	0.0140

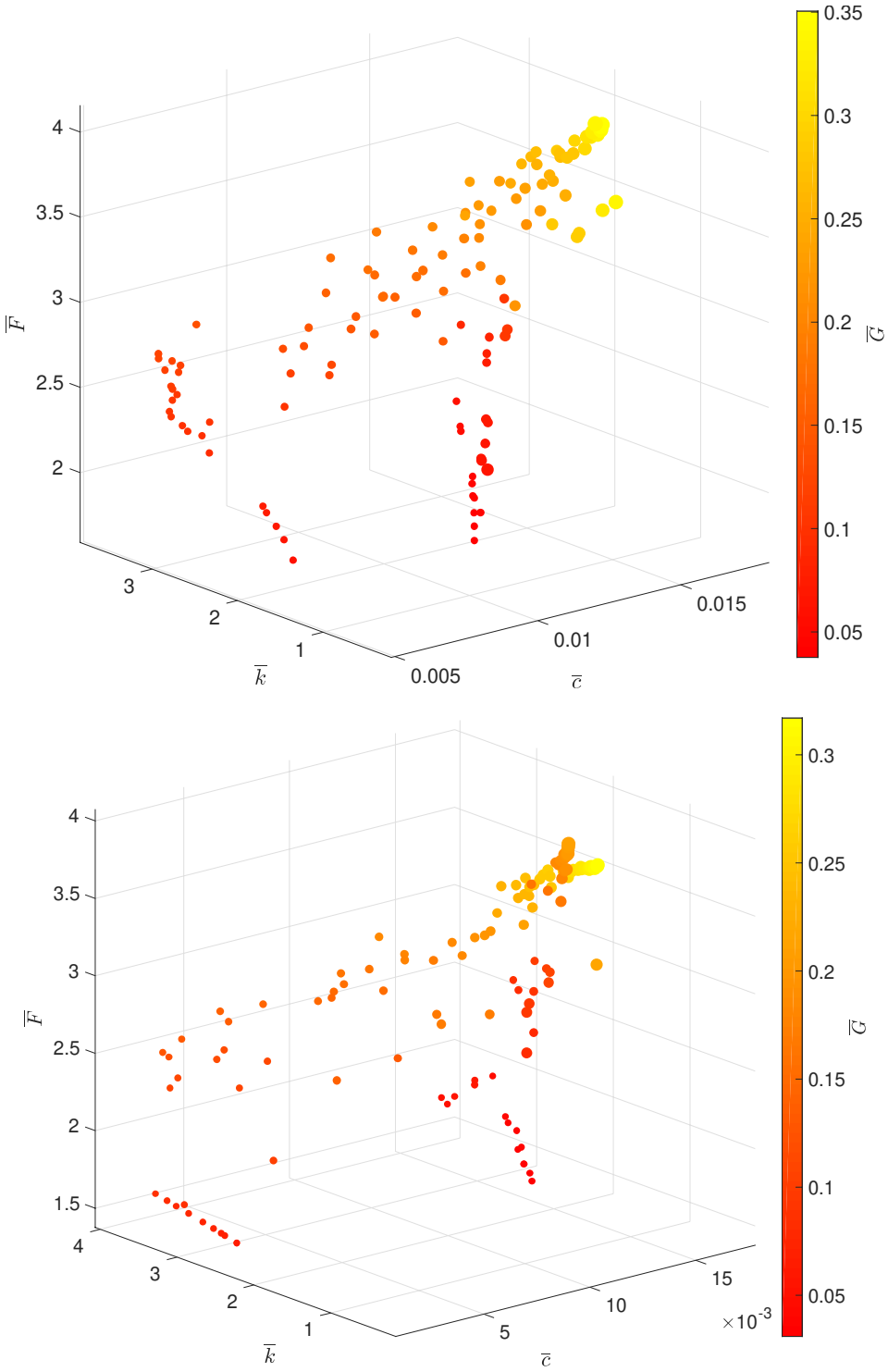

Fig. 3 4D Pareto front (top: central hole forced; bottom: central hole not forced). Dot colouring refers to air consumption; dot size proportional to average diameter size of the holes.

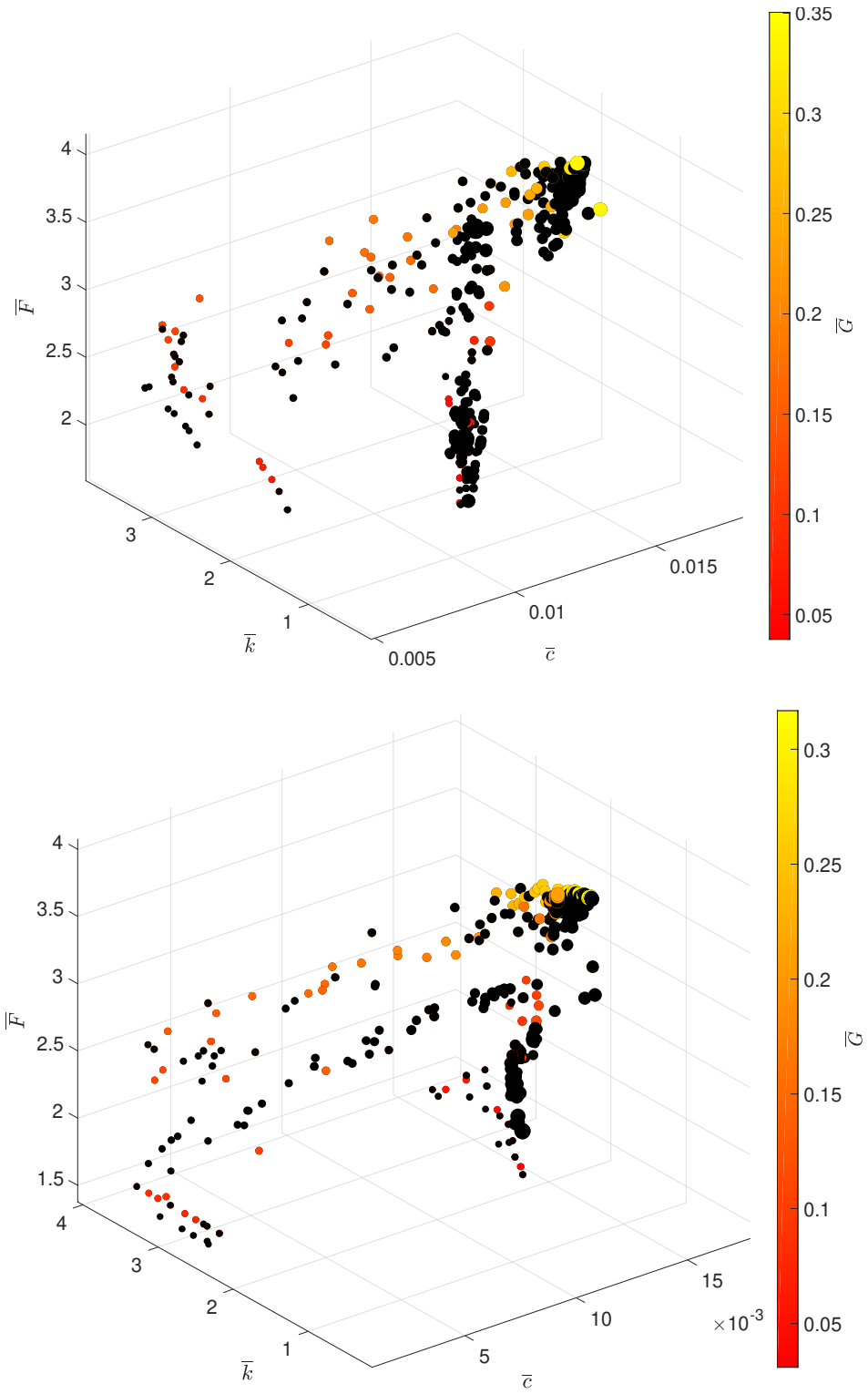

Fig. 4 4D Pareto front (top: central hole forced; bottom: central hole not forced) with also non-optimal individuals (in black).

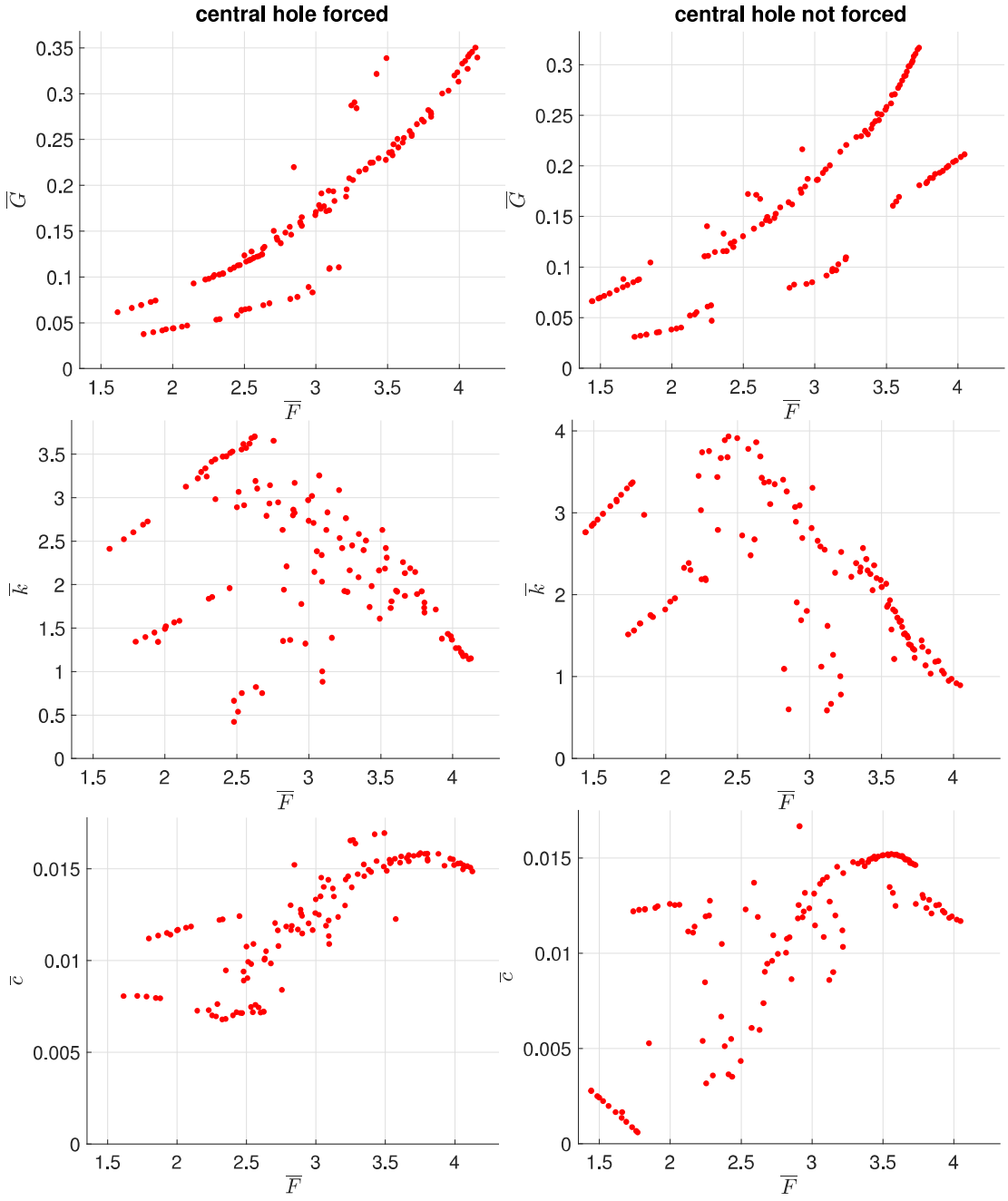

Fig. 5 Projection on 2D planes of the Pareto front with central hole forced (left) or not forced (right).

It is possible to notice that the disposition of holes of configurations 85 and 111 is very similar, apart four holes, but the mean diameter is different. Due to the greater mean diameter (+16%), in configuration 111 at $\overline{h}$= 0.8 the load capacity, the damping capability and the air consumption are increased of 10%, 21% and 28% respectively, while stiffness is decreased of 17%. Comparing config. 85 with config. 103, the number of holes and their mean diameter are approximately the same, but their disposition in config. 103 is moved towards the center of the pad. As a result of this, the air consumption decreases (-50%), but also the stiffness (-52%). The decreased air flow can be explained by the higher pneumatic resistance between holes and the edges of the pad, whereas the decreased stiffness can be explained by the lower sensitivity of the pressure distribution with respect to the air gap.

Considering the second case (central hole not forced), configurations 21, 29, 34 and 118 are selected at a supply pressure near 6 bar. Table 2 lists the data on geometry and on the objective functions, while Figure 8 depicts the holes dispositions and Figure 9 represents the objective functions vs the air gap $\overline{h}$.

Table 2 Example of comparison of four configurations at similar supply pressure, with central hole not forced.

Configuration	**21**	**29**	**34**	**118**
Mean diameter $\bar{d}$	0.53	1.26	0.57	0.50
Standard deviation	0.02	0.17	0.05	0
Number of holes	26	36	26	30
Supply pressure (bar)	5.997	5.982	6.035	6.031
Load capacity $\bar{F}$ (at $\bar{h} = 0.8$)	2.172	3.149	2.249	1.615
Airflow $\bar{G}$ (at $\bar{h} = 0.8$)	0.055	0.097	0.061	0.077
Stiffness $\bar{k}$ (at $\bar{h} = 0.8$)	2.30	0.67	2.19	3.08
Damping $\bar{c}$ (at $\bar{h} = 0.8$)	0.0114	0.0090	0.0118	0.0017

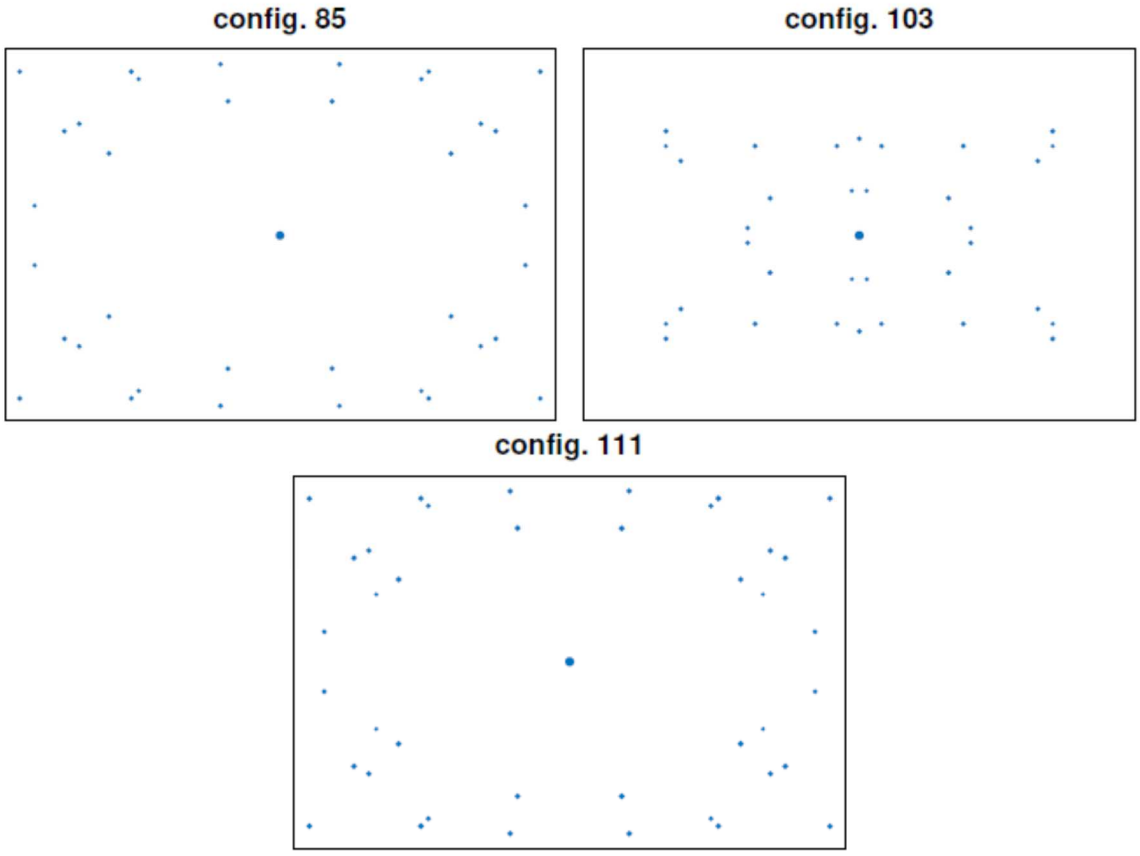

Fig. 6 Holes disposition of the example configurations listed in Table 1.

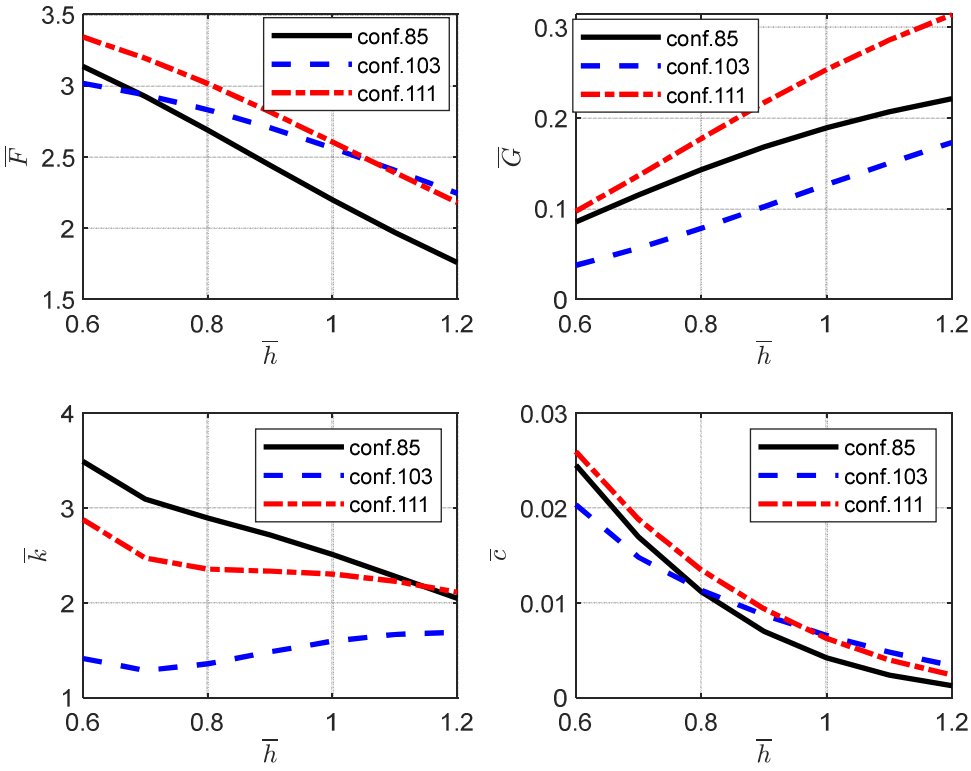

Fig. 7 Static and dynamic characteristics of the example configurations listed in Table 1; coefficients k (stiffness) and c (damping) are calculated at f = 100 Hz.

Configurations 21 and 34 have exactly the same holes disposition; only the mean diameter of the supply holes changes. Load capacity, air consumption and damping are slightly increased (+3.5%, +11% and +3.5% respectively) due to the slight increase of the mean diameter (+7.5%). Stiffness is slightly decreased (-5%). The static characteristics vs the air gap are very similar, with also the dynamic coefficients of stiffness and damping, calculated at f = 100 Hz. In config. 118 all supply holes have a diameter coincident with the lower bound. If compared with config. 21, which has a similar mean diameter of supply holes, the air consumption is greater, while the load capacity and the damping coefficient are much lower. Stiffness is very high, due to the distribution of the supply holes, very near to the edges of the pad. Anyway, the stiffness sensitivity respect to the air gap is very high, while for configs. 21, 29 and 34 stiffness is little sensitive to the air gap. This is because while in these three configs. the holes are positioned far from the edges of the pad, in config. 118 the holes are positioned near the edges. Configuration 29 has greater mean diameter (+138%) and number of supply holes (+38%) than configuration 21; for this reason, the load capacity and the air consumption are greater (+45% and +43% respectively). The stiffness coefficient is much lower (-71%) while the influence on damping capability is not always the same, as it depends on the air gap value. Anyway, the different disposition of the supply holes between configs. 29 and 21 could influence this comparison.

4.3. Effect of the supply pressure

In Figure 10 all points of the Pareto front are reported versus the supply pressure in case of central hole imposed. The effect of the supply pressure on the objective functions is not so evident, as also other parameters such as the mean diameter and the number of the supply holes influence them. Anyway, it is well known that increasing the supply pressure all the objective functions increase, and this trend is confirmed from the graphs.

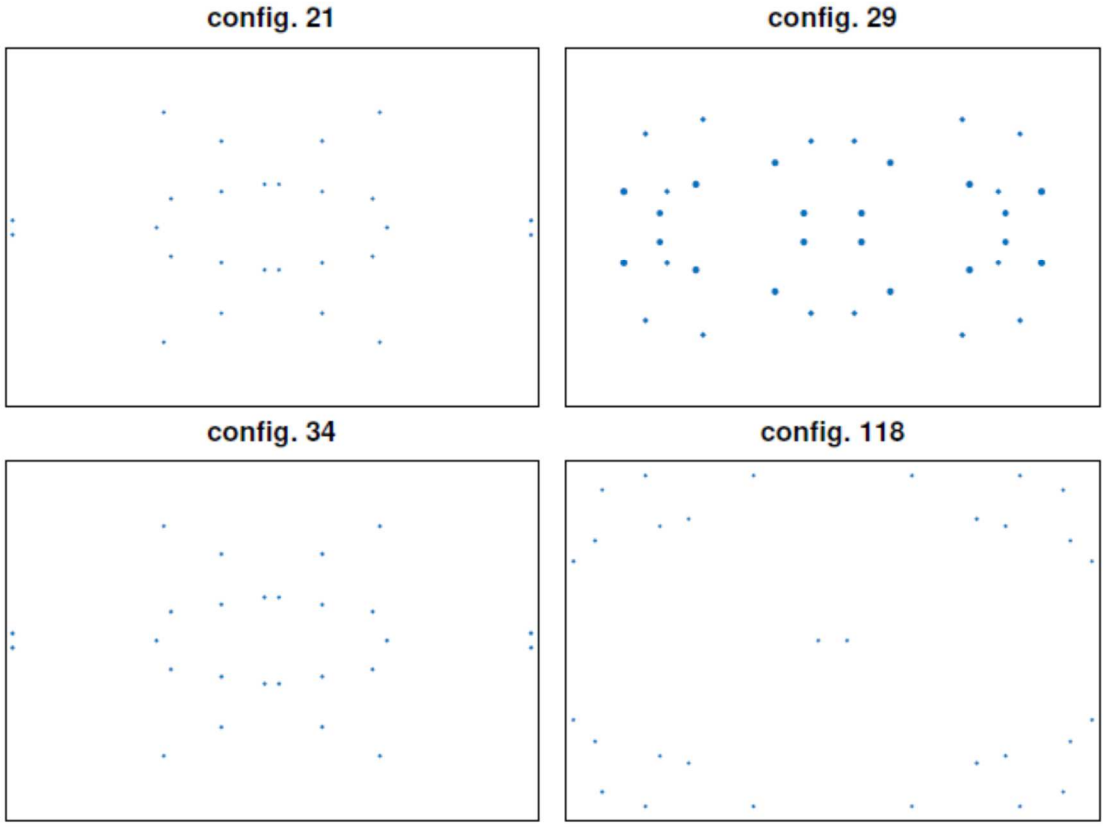

Fig. 8 Holes disposition of the example configurations listed in Table 2.

4.4. Effect of the mean holes diameter

Figure 11 shows the effect of the average supply holes diameter on the objective functions, calculated at $\bar{h}$= 0.8: increasing it, load capacity, air flow and damping are increased, while stiffness generally is decreased. Stiffness could increase in some cases at high air gaps, when the load capacity is compromised by excessively small orifices.

4.5. Considerations on the supply holes number

Table 3 indicates the number of the supply holes of the configurations obtained in the last population by the genetic algorithm. It is worth noting that in the Pareto set there are no configurations with a number of supply holes lower than 24. The holes number is far from the bounds defined (N_{min} = 4, N_{max} = 60). This means that in order to design an optimised pad with multiple supply holes, 4 holes are too few and 60 holes are too many.

Table 3 Occurrences of configurations in the Pareto front with a given number of supply holes.

Central hole forced		Central hole not forced	
Num. of holes	*Num. of Pareto solutions*	*Num. of holes*	*Num. of Pareto solutions*
31	5	24	10
33	23	26	5
35	9	30	13
37	46	32	7
39	1	34	43
41	36	36	11
45	3	38	17
-	-	40	17

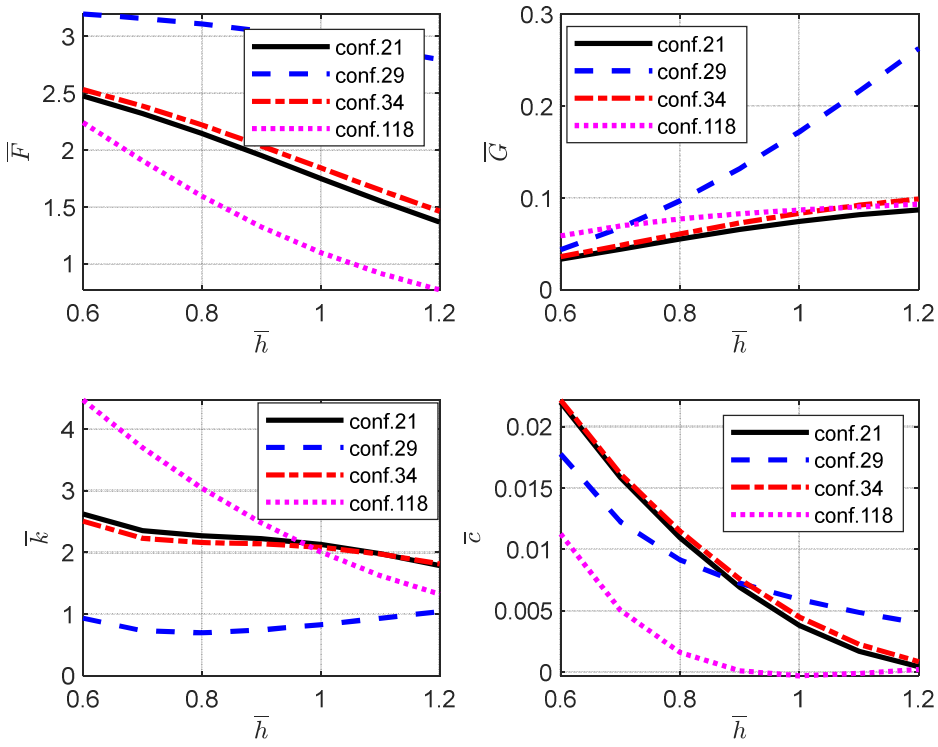

Fig. 9 Static and dynamic characteristics of the example configurations listed in Table 2; coefficients k (stiffness) and c (damping) are calculated at $f = 100$ Hz.

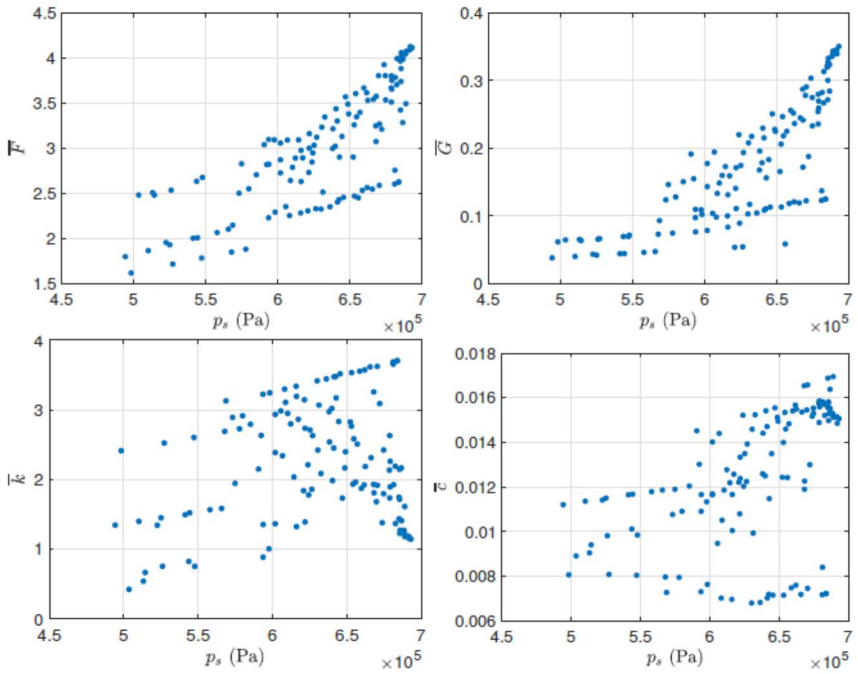

Fig. 10 Objective functions versus supply pressure p_s (central hole forced).

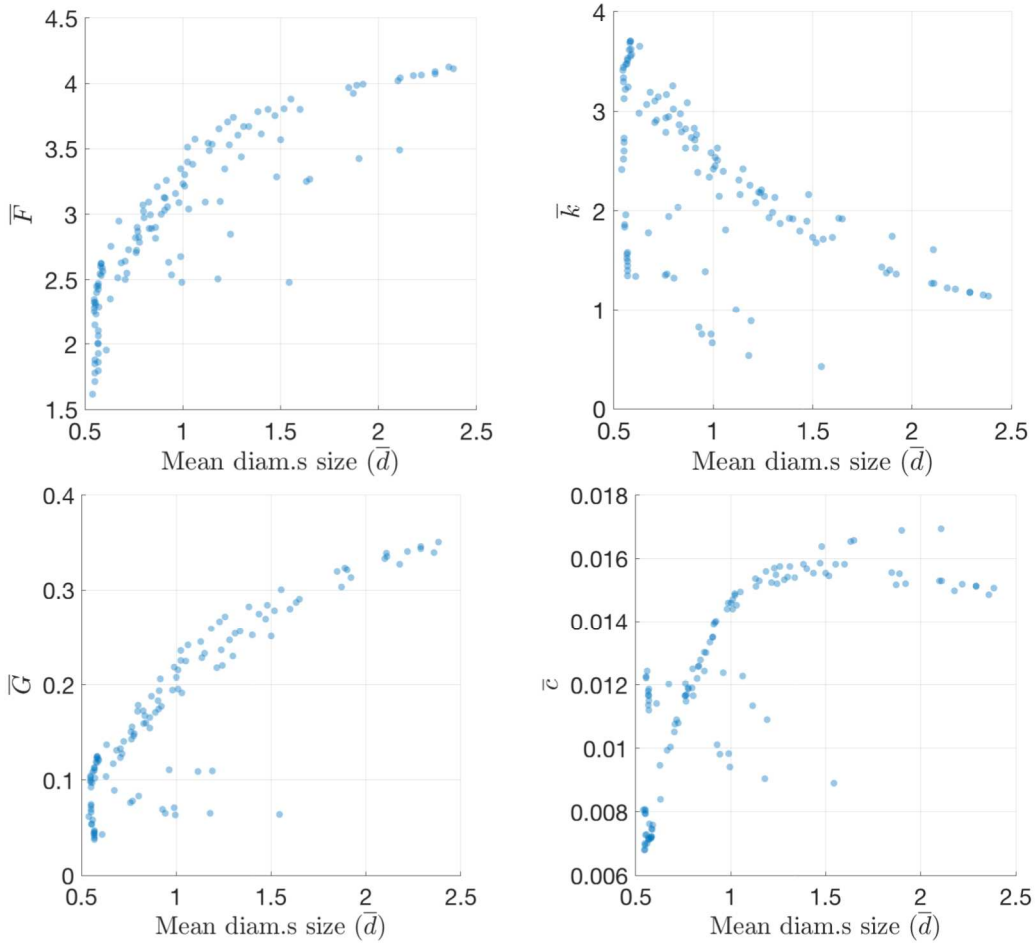

Fig. 11 Objective functions versus the mean supply holes diameter d_s (central hole forced).

5. CONCLUSIONS

The paper presents an optimisation approach for multiple orifices aerostatic pad which involves the possibility to consider also number and disposition of the holes as a design parameter, without a pre-defined scheme. In order to consider the holes location in the design variable of the optimizer, creation, mutation and crossover functions have been written. The optimisation process defines a set of optimal solutions in the Pareto front. Depending on the application, the designer can select a solution giving priority to some objective functions with respect to others, e.g. giving more importance to the load capacity maximization or to the stiffness coefficient maximization.

The effect of the design parameters has been discussed and the following conclusions can be drawn:

- on the Pareto front there is an evident relationship between the objective function behaviours;
- on the Pareto front damping coefficient increases together with load capacity and air consumption, while stiffness is maximum at average load capacities;
- on the Pareto front there are no configurations with less than 24 supply holes;
- increasing the mean diameter of the supply holes entails an increase of load capacity, damping capability and air consumption;
- stiffness can be increased reducing the mean diameter of the supply holes; anyway this is not always true, especially at high air gaps in case the orifice diameter is too small;
- moving the supply holes towards the center i) increases the load capacity and makes the pad more performing at high air gaps, as the load capacity decrement is lower with respect to configurations with supply holes near the edges; ii) reduces air consumption and stiffness; iii) reduces the stiffness sensitivity respect to the air gap.

In a future work, authors intend to perform multiobjective optimisations considering a fixed supply pressure and only two objective functions, like e.g. (f_1, f_4), (f_2, f_4), or (f_3, f_4) in order to compare the optimisation results with those obtained considering all four objectives.

ACKNOWLEDGEMENTS

Research performed in the framework of the Italian MIUR Award Dipartimento di Eccellenza 2018-2022 to the Department of Mathematical Sciences, Politecnico di Torino, CUP: E11G18000350001. The research leading to these results has also been partially funded by INdAM-GNCS and by the SmartData@PoliTO center for Big Data and Machine Learning technologies.

NOMENCLATURE

h	air gap height, m;
k	pad stiffness, N/m;
$f_1 \div f_4$	objective functions;
F	pad load capacity, N;
c	pad damping coefficient, Ns/m;
p	pressure, Pa;
p_c	supply holes downstream pressure, Pa;
p_s	pad supply pressure, Pa;
p_a	ambient pressure, Pa;
μ	dynamic air viscosity, kg/(m·s);
t	time, s;
R	gas constant, J/(kg·K);
G	mass air flow, kg/s;
c_d	discharge coefficient of the supply hole;
T	absolute temperature, K;
d_s	supply holes diameter, m;
k_T	temperature ratio;
ϕ	pressure ratio;
ω	perturbation frequency, rad/s;
φ	phase lag between force and air gap, rad;
N	number of supply holes;

REFERENCES

1. Huang, H. C., Al-Bender, F. and Van Brussel, H., "Optimum design of inherently compensated aerostatic thrust bearings", in Kals, H. and Van Houten, F., "*Integration of Process Knowledge into Design Support Systems*", Springer, Dordrecht (1999). https://doi.org/10.1007/978-94-017-1901-8 17.
2. Sescu, A., Sescu, C., Dimofte, F., Cioc, S., Afjeh, A. A. and Handschuh, R., "A study of the steady-state performance of a pressurized air wave bearing at concentric position", *Tribology Transactions*, **52**(4), pp.544-552 (2011). https://doi.org/10.1080/10402000902774275.
3. Lu, C. J., Chiou, S. S. and Wang, T. K., "Adaptive multilevel method for the air bearing problem in hard disk drives", *Tribology International*, **37**(6), pp.473-480, (2004). ISSN 0301-679X, https://doi.org/10.1016/j.triboint.2004.01.001.
4. Wang, N., Tsai, C. M. and Cha, K. C., "Optimum design of externally pressurized air bearing using cluster openMP", *Tribology International*, **42**(8), pp.1180-1186 (2009). ISSN 0301-679X, https://doi.org/10.1016/j.triboint.2009.03.016.

5. Wang, N. and Cha, K. C., "Multi-objective optimization of air bearings using hypercube-dividing method", *Tribology International*, **43**(9), pp.1631-1638 (2010). ISSN 0301-679X, https://doi.org/10.1016/j.triboint.2010.03.009.

6. Hashimoto, H. and Ochiai, M., "Optimization of groove geometry for thrust air bearing to maximize bearing stiffness". *ASME. J. Tribol.*, **130**(3), pp.031101--031101-11 (2008). https://doi.org/10.1115/1.2913546.

7. Schiffmann, J. J., "Integrated design and multi-objective optimization of a single stage heat-pump turbocompressor", *ASME. J. Turbomach.*, **137**(7), pp.071002--071002-9 (2015). https://doi.org/10.1115/1.4029123.

8. Schiffmann, J. J. and Favrat, D. D., "Integrated design and optimization of gas bearing supported rotors", *ASME. J. Mech. Des.*, **132**(5), pp.051007--051007-11 (2010). https://doi.org/10.1115/1.4001381.

9. Zhu, H. and Bogy, D. B., "Hard disc drive air bearing design: modified direct algorithm and its application to slider air bearing surface optimization", *Tribology International*, **37**(2), pp.193-201 (2004). ISSN 0301-679X, https://doi.org/10.1016/S0301-679X(03)00036-7.

10. Zhang, J. and Talke, F. E., "Optimization of slider air bearing contours using the combined genetic algorithm subregion approach", *Tribology International*, **38**(6-7), pp.566-573 (2005). ISSN 0301-679X, https://doi.org/10.1016/j.triboint.2005.01.013.

11. Jayson, E. M. and Talke, F. E., "Optimization of air bearing contours for shock performance of a hard disk drive", *ASME. J. Tribol.*, **127**(4), pp.878-883 (2005). https://doi.org/10.1115/1.2000979.

12. Kotera, H. and Shima, S., "Shape optimization to perform prescribed air lubrication using genetic algorithm", *Tribology Transactions*, **43**(4), pp.837-841 (2008). https://doi.org/10.1080/10402000008982416.

13. Holland, J. H., *Adaptation in Natural and Artificial Systems*, University of Michigan Press, Ann Arbor (1975).

14. Schaffer, J. D. “Multiple Objective optimization with vector evaluated genetic algorithms”, *International Conference on Genetic Algorithm and their applications: Proceedings of the First International Conference on Genetic Algorithms*, pp. 93-100, 1985.

15. Fonseca, C. M. and Fleming, P. J. “Multiobjective genetic algorithms”, *Proceedings of IEE Colloquium on `Genetic Algorithms for Control Systems Engineering* (Digest No. 1993/130), 28 May 1993. 1993. London, UK: IEE.

16. Fonseca, C. M. and Fleming, P. J., “Genetic algorithms for multiobjective optimization: formulation, discussion and generalization”, *Proceedings of ICGA-93: Fifth International Conference on Genetic Algorithms*, 17-22 July 1993. 1993. Urbana Champaign, IL, USA: Morgan Kaufmann.

17. Coello, C. A. C., “A comprehensive survey of evolutionary-based multiobjective optimization techniques”, *Knowledge and Information Systems,* **1**(3), pp. 269-308 (1999).

18. Zitzler, E. and Thiele, L., “Multiobjective evolutionary algorithms: a comparative case study and the strength Pareto approach”, *IEEE Transactions on Evolutionary Computation,* **3**(4), pp. 257-271 (1999).

19. Zitzler, E., Deb, K., and Thiele, L., “Comparison of multiobjective evolutionary algorithms: empirical results”, *Evolutionary Computation,* **8**(2), pp. 173-195 (2000).

20. Sarker, R., Liang, K.-H., and Newton, C., “A new multiobjective evolutionary algorithm”, *European Journal of Operational Research,* **140**(1), pp. 12-23 (2002).

21. Deb, K., Pratap, A., Agarwal, S., and Meyarivan, T., “A fast and elitist multiobjective genetic algorithm: NSGA-II”, *IEEE Transactions on Evolutionary Computation,* **6**(2), pp. 182-197 (2002).

22. Lu, H. and Yen, G.G., “Rank-density-based multiobjective genetic algorithm and benchmark test function study”, *IEEE Transactions on Evolutionary Computation,* **7**(4), pp. 325-343 (2003).

23. Wang, N., "A parallel computing application of the genetic algorithm for lubrication optimization", *Tribology Letters*, **18** (2005). https://doi.org/10.1007/s11249-004-1763-x.

24. Schiffmann, J. J. and Favrat, D. D., “Multi-objective optimisation of herringbone grooved gas bearings supporting a high speed rotor, taking into account rarefied gas and real gas effects”, *ASME Engineering Systems Design and Analysis, Volume3: Dynamic Systems and Controls*, Symposium on Design and Analysis of Advanced Structures, and Tribology, pp.857-865. https://doi.org/10.1115/ESDA2006-

95085.

25. Lu, C. and Wang, T., "New designs of HDD air-lubricated sliders via topology optimization", *ASME. J. Tribol.*, **126**(1), pp.171-176 (2004). https://doi.org/10.1115/1.1631016.
26. Wang, N. and Chang, Y. Z., "A hybrid search algorithm for porous air bearings optimization", *Tribology Transactions*, **45**(4), pp.471-477 (2008). https://doi.org/10.1080/10402000208982576.
27. Zhong, W., Li, X., Tao, G. and al., "Theoretical and experimental investigation on optimization of a non-contact air conveyor", *J. Cent. South Univ*. (2016). https://doi.org/10.1007/s11771-016-3080-6.
28. Lu, S., Hu, Y., O'Hara, M., Bogy, D. B., Singh Bhatia, C. and Yiao-Tee Hsia, "Air bearing design, optimization, stability analysis and verification for sub-25 nm flying", *IEEE Transactions on Magnetics*, **32**(1), pp.103-109 (1996). https://doi.org/10.1109/20.477558.
29. Yoon, S. and Choi, D., "An optimum design of the transverse pressure contour slider for enhanced flying characteristics", *ASME. J. Tribol.*, **119**(3), pp.520-524 (1997). https://doi.org/10.1115/1.2833531.
30. Hong Zhu and Bogy, D. B., "Direct algorithm and its application to slider air-bearing surface optimization", *IEEE Transactions on Magnetics*, **38**(5), pp.2168-2170 (2002). https://doi.org/10.1109/TMAG.2002.802794.
31. Bhat, N. and Barrans, S. M., "Design and test of a Pareto optimal flat pad aerostatic bearing", *Tribology International*, **41**(3), pp.181-188 (2008). https://doi.org/10.1016/j.triboint.2007.07.011.
32. Bhat, N., Barrans, S. M. and Kumar, A. S., "Performance analysis of Pareto optimal bearings subject to surface error variations", *Tribology International*, **43**(11), pp.2240-2249 (2010). ISSN 0301-679X, https://doi.org/10.1016/j.triboint.2010.07.012.
33. Colombo, F. and Conte, M., "Multi-objective optimization of a rectangular air bearing by means of genetic algorithms", *Journal of Mechanics Engineering and Automation*, **2**, pp.355-364 (2012).
34. Colombo, F., Lentini, L., Raparelli, T., Trivella, A. and Viktorov, V., "Dynamic characterisation of rectangular aerostatic pads with multiple inherent orifices", *Tribology Letters*, pp.66-133 (2018). https://doi.org/10.1007/s11249-018-1087-x.
35. Belforte, G., Colombo, F., Raparelli, T., Trivella, A. and Viktorov, V., "Experimental analysis of air pads with micro holes", *Tribology Transactions*, **56**(2), pp.169-177 (2013).
36. "*Global Optimization Toolbox User's Guide*", The MathWorks, Inc., chapter 9.
37. "*Global Optimization Toolbox User's Guide*", The MathWorks, Inc., chapter 11.

Fig. 1 5 points stencil around the control volume centered in (i,j).

Fig. 2 Example of Pareto optimal solutions. Red dots: optimal solutions (Pareto Front); black dots: non-optimal points.

Fig. 3 4D Pareto front (top: central hole forced; bottom: central hole not forced). Dot colouring refers to air consumption; dot size proportional to average diameter size of the holes.

Fig. 4 4D Pareto front (top: central hole forced; bottom: central hole not forced) with also non-optimal individuals (in black).

Fig. 5 Projection on 2D planes of the Pareto front with central hole forced (left) or not forced (right).

Fig. 6 Holes disposition of the example configurations listed in Table 1.

Fig. 7 Static and dynamic characteristics of the example configurations listed in Table 1; coefficients k (stiffness) and c (damping) are calculated at $f = 100$ Hz.

Fig. 8 Holes disposition of the example configurations listed in Table 2.

Fig. 9 Static and dynamic characteristics of the example configurations listed in Table 2; coefficients k (stiffness) and c (damping) are calculated at $f = 100$ Hz.

Fig. 10 Objective functions versus supply pressure p_s (central hole forced).

Fig. 11 Objective functions versus the mean supply holes diameter d_s (central hole forced).